ELSEVIER

S0032-3861(96)00387-4

Polymer Vol. 37 No. 24, pp. 5357–5365, 1996

0032-3861/96/$15.00 + 0.00

SAXS studies of lamellar level morphological changes during crystallization and melting in PEEK

Ravi K. Verma*, Vesselin Velikov*, Ronald G. Kander† and Herve Marand*†‡

**Department of Chemistry and †Department of Materials Science and Engineering, NSF Science and Technology Center for Polymeric Adhesives and Composites, Virginia Polytechnic Institute and State University, Blacksburg, VA 24061, USA*

and Benjamin Chu

Department of Chemistry, State University of New York at Stony Brook, Stony Brook, New York, USA

and Benjamin S. Hsiao‡

DuPont CR&D, Experimental Station, E.I. DuPont de Nemours & Co., Wilmington, DE 19880-0302, USA

(Received 29 September 1995; revised 24 January 1996)

The double endothermic behaviour of poly(aryl ether ether ketone) (PEEK) has been the subject of considerable debate during the last few years. In this paper, the various explanations for the double endothermic behaviour of PEEK are examined using a combination of real time small angle X-ray scattering (SAXS) and differential scanning calorimetry (d.s.c.) techniques. The correlation function approach was used to analyse SAXS data. The correlation functions were interpreted in terms of a two-phase model to obtain average lamellar and amorphous layer thicknesses. The average lamellar and amorphous layer thicknesses are observed to be about 125 Å and 50 Å respectively. From the SAXS data, it is observed that the average amorphous layer thickness (1) does not decrease during the development of the low endotherm, and (2) decreases during melting at temperatures corresponding to the low endotherm. From the d.s.c. studies, it is observed that the high endotherm develops before the low endotherm. Based on these and other observations, the melting recrystallization model and the lamellar insertion model are ruled out as possible explanations for the origin of the low endotherm in PEEK. We suggest that the origin of the low and high endotherms lies in melting of secondary and primary lamellar stacks respectively. The secondary lamellar stacks consist of thinner lamellae and thicker amorphous layers as compared to the primary lamellae which results in the high endotherm.

(Keywords: real time SAXS; synchrotron radiation; correlation function)

INTRODUCTION

The dual endothermic behaviour observed in poly(aryl ether ether ketone) (PEEK) has been the subject of some controversy in the last few years. Several authors have reported the occurrence of a low endotherm in PEEK in addition to the higher temperature melting endotherm (at about 330–350°C)[1–8]. This low endotherm normally occurs at about 5 to 30°C above the crystallization temperature, increases in magnitude and shifts to higher temperature with increasing crystallization/annealing temperature or time. Blundell and Osborn[2,3], and Lee and Porter[4,5] have accounted for this phenomenon by a melting recrystallization process. Cheng *et al.*[6] have stated that it is the result of an annealing process. On the other hand Cebe and Hong[7] and Bassett *et al.*[8] have suggested that the double endothermic behaviour is associated with the melting of a bimodal distribution of crystalline lamellar thicknesses. They suggest that melting of thinner lamellae is manifested in the low endotherm and the thicker lamellae in the high endotherm.

Several authors[9–13] have used the real time small angle X-ray scattering (SAXS) measurements to suggest that the low endotherm is caused by the melting of thinner lamellae inserted between layers of thicker lamellae, and that the higher temperature endotherm is caused by melting of the remaining lamellae. This model (referred to as the lamellar insertion model) is an extension of the dual population model. For example, Hsiao *et al.*[9,10] have reported observing a decrease in long periods during the initial stages of crystallization. They explain this observation by suggesting that thinner

‡ To whom correspondence should be addressed

lamellae are inserted between two layers of thicker primary lamellae[11]. However, they have also presented data[11] which suggest that the interlamellar amorphous layer thickness remains about constant during melting. (In ref. 11, a comparison of Figures 11 and 14 clearly shows that L_B and l_c have similar trends, suggesting that l_a (the difference between them) is about constant.) Wang *et al.*[12] have also used real time SAXS techniques to suggest a similar mechanism for the low endotherm. Krüger and Zachmann[13] have employed differential scanning calorimetry (d.s.c.) techniques along with a combination of real time SAXS and wide angle X-ray diffraction (WAXD) techniques to study the melting of PEEK. They observe a more rapid decrease in the WAXD apparent degree of crystallinity A_c, compared to the SAXS invariant Q. Following their argument, melting of whole lamellar stacks would have decreased the invariant and the degree of crystallinity equally. Therefore, they conclude that the lower endotherm is caused by partial melting within a lamellar stack rather than the melting of complete lamellar stacks. However, their argument assumes that melting of separate stacks would not affect the average lamellar and amorphous layer thickness of the remaining stacks. They have not estimated the lamellar and amorphous layer thickness to test for this assumption. Any changes in the average amorphous and lamellar thicknesses would affect the value of the scattering invariant Q. Further, they have not corrected their apparent degree of crystallinity (A_c) for changes in the Debye–Waller factor with temperature. Jonas *et al.*[14] have demonstrated that this change can be substantial over the temperature range of interest. Lattimer *et al.*[15] have used transmission electron microscopy (TEM) techniques to observe the melting of thinner lamellae at temperatures corresponding to the lower endotherm. They have observed thinner lamellae present in separate stacks in addition to some found between layers of thicker lamellae. Their work clearly demonstrates that the lamellar insertion model suggested by several authors[9–13] is probably incomplete when used to explain the low endotherm. More recent work by Velikov and Marand[16] demonstrated that the kinetics of the development of the low endotherms resembles the kinetics of an enthalpic relaxation process. Based on this and other observations, they suggested that the origin of the low endotherm lies in the enthalpic recovery of a 'rigid amorphous fraction'. However, Krüger and Zachmann have also calculated the rate of change of the crystallinity index A_c (estimated by WAXD) with temperature during melting. They show that the dA_c/dT plot resembles the d.s.c. scan during melting. This resemblance clearly indicates that the low endotherm is indeed associated with a melting type process.

Irrespective of whether the low endotherm is associated with a dual population of lamellae, there is still a lack of detailed understanding of the spatial distribution of these lamellae within PEEK spherulites. Optical microscopy studies by Marand and Prasad[17] suggest infilling at long times at the edges of spherulites crystallized at relatively high temperatures ($T >$ 295°C). Lovinger and Davis[18] have studied the morphology of PEEK crystallized from solution at relatively high temperatures (in benzophenone at about 225°C and in α-chloronaphthalene at about 213°C) using TEM techniques. They observed two types of morphology for spherulites crystallized at high temperatures (benzophenone at 220°C) and only one for spherulites crystallized at lower temperatures (210°C). They have observed some thinner fibrous lamellae and have demonstrated that both types possess the same crystal structure and growth directions. Lovinger *et al.*[19] have also studied the morphology of PEEK melt crystallized at relatively high temperatures (310–320°C). Unlike Marand and Prasad, they have not studied the evolution of the morphology with time. However, they suggest that the more birefringent regions observed by Marand and Prasad are associated with thick stacks of lamellar crystals. The occurrence of such stacks decreases with decreasing crystallization temperature in such a way that isolated dominant lamellae grow at lower temperatures ($T <$ 300°C). Their observation suggests that for melt crystallization, infilling of secondary lamellae occurs between stacks at high crystallization temperatures and between primary lamellae at lower crystallization temperatures. Clearly, a detailed morphological picture of the semicrystalline material has not emerged. However, the work of Lovinger and Davis, and of Marand and Prasad suggests that the actual morphology consists of stacks of crystalline lamellae separated by amorphous regions of significant dimensions.

In this study, we will address the following two questions. (1) Are the lamellae (dominant and secondary) uniformly distributed in the spherulites or do they exist in separate stacks of thick dominant and thin infilling lamellae? (2) Can we unambiguously prove or disprove the various models that have been proposed for the low endotherm? To these ends, time resolved SAXS measurements are performed on PEEK to monitor the morphological changes during crystallization and melting. A high crystallization temperature (307°C) is chosen for this study. This crystallization temperature was selected so as to ensure the formation of lamellar stacks. The raw SAXS data will be analysed using the correlation function[20] approach.

The long period (L_c^M), lamellar thickness (l_c), amorphous layer thickness (l_a) and linear degree of crystallinity (X_{cl}) are calculated from the correlation functions. The invariant (Q) is calculated from the Lorentz corrected intensity profile. The above morphological parameters are monitored during crystallization and melting and examined in the light of the d.s.c. results.

EXPERIMENTAL

Sample preparation

PEEK samples used in this study were kindly donated by ICI Inc. (PEEK 450G in pellet form). For the SAXS measurements, disc-like samples (7 mm in diameter and 1.5 mm thick) were prepared in a hot press. First, all the samples were dried in vacuum at 140°C for 24 h. The polymers were then weighed and melted in a suitable steel mould at 385°C for 4 min without any platen pressure. After the 4 min hold, water cooling was applied to the whole system ($\sim 60°C\,min^{-1}$) while the pressure was gradually increased on the sample. (Samples were visually inspected for porosity and crystallinity. Samples with relatively high crystallinity were rejected because they could not be visually inspected for macroscopic voids. Only void-free samples were used.)

D.s.c. and real time SAXS measurements

D.s.c. measurements were performed either on a Seiko system capable of cooling at 200°C min^{-1} or on a Perkin Elmer System DSC System 2C capable of cooling at 320°C min^{-1}. In all cases, the samples were melted at 385°C for 4 min under a dry nitrogen purge.

Real time SAXS measurements were carried out at the SUNY X3A2 beamline at the National Synchrotron Light Source (NSLS) at the Brookhaven National Laboratory. Detailed descriptions of the set-up have been provided in previous publications[9,10]. Briefly, the data were collected using a modified Kratky optics (sample to detector distance = 500 nm, beam size of 1.5 × 0.2 mm, $\lambda = 1.54$ Å) and a linear position sensitive detector (EG&G, PARC, model 1453) in the angular range of $2\theta = 0$ to 1.5°. For melt crystallization, the samples were initially equilibrated above the melting temperature (385°C) for 4 min in one chamber and then moved to another chamber at the crystallization temperature (305–307°C) using a pneumatic piston. a specially designed 'temperature jump unit'[9,10] was used for this purpose. The time to reach and equilibrate at the crystallization temperature was estimated to be about 30 s. Relatively long data collection times were employed (50 s) so as to ensure greater signal to noise ratios at the expense of time resolution.

SAXS data analysis

The measured raw SAXS data were corrected for parasitic scattering. The relatively long data collection times resulted in a reasonable signal to noise ratio and obviated the need for any data smoothing. Further, the modified Kratky optics was assumed to approximate pinhole collimation and no desmearing was performed on the data. Such an assumption has been previously shown to be justified for our set-up[9,10]. *Figure 1a* depicts SAXS profiles (I–q plots) of a PEEK sample for different crystallization times. *Figure 1b* depicts the Lorentz corrected SAXS profiles. The one-dimensional correlation function was calculated from the corrected SAXS data. The correlation function is the Fourier transform of the corrected SAXS data as given in equation (1):

$$\gamma_1(r) = \frac{\int_0^\infty [I - I_b]q^2 \cos(qr)\mathrm{d}q}{\int_0^\infty [I - I_b]q^2 \mathrm{d}q} \quad (1)$$

where $\gamma_1(r)$ is the one-dimensional correlation function, I_b is the contribution to scattering from local electron density fluctuations in the amorphous phase (liquid scattering) and q is the scattering vector given by:

$$q = \frac{4\pi}{\lambda}\sin[\theta] \quad (2)$$

where 2θ is the scattering angle.

Before the Fourier transformation can be performed, the data have to be extrapolated to high and low q values. The data were extrapolated to low q values (in the beam stop region) assuming a linear $[I - I_b]q^2$ *versus* q^2 profile. The extrapolation in the high q region was more problematic due to a lower signal to noise ratio and because of the relatively small angular range used. This extrapolation was done with the aid of Porod's law[21]

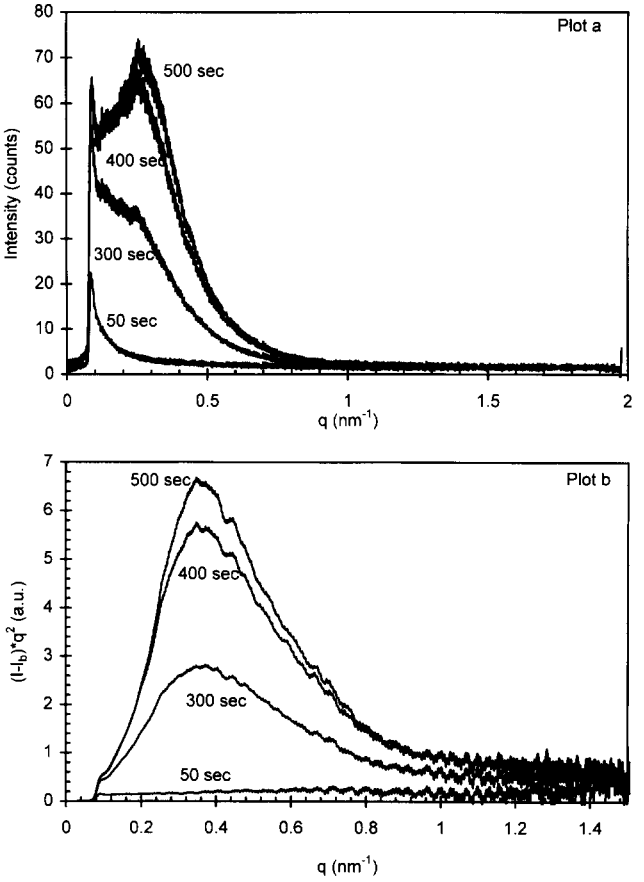

Figure 1 The evolution of the SAXS pattern during crystallization. (a) Raw SAXS data and (b) the corresponding Lorentz corrected plots. Lorentz correction was performed after subtracting the liquid scattering profile as discussed in the text

(depicted in equation (3)).

$$\lim_{q\to\infty}[K - (I - I_b)q^4 \exp(\sigma^2 q^2)] = 0 \quad (3)$$

where K is a Porod law constant, and σ is a constant related to the width of the crystal amorphous transition zone. Note that the calculated correlation functions are dependent on the estimated values of I_b, K and σ. The estimates of I_b, K and σ are not exact because of the absence of a true Porod regime in the scattering data (see *Figures 2a* and *2b*). Collecting data over a larger angular range (e.g. 0–4°) would probably have yielded a true Porod regime and would also possibly have enabled the exact calculation of a polynomial type expression for I_b. Given the small angular range, the Bonart and Müller[22] type expression for I_b was assumed and no attempt was made to model the Vonk[23] type polynomial ($I_b(q) = C + bq^n$, where n is an even integer and C is a constant) or the Ruland[24] type exponential ($I_b(q) = C\exp(aq^2)$) form of I_b. Also, the interfacial thickness (as analysed by equation (3)) cannot be reported with greater accuracy because of the small angular range used. In general, the interfacial thickness calculated from equation (3) was in the range of 15–20 Å for all PEEK samples. Koberstein and Stein[21] have demonstrated that values of the interfacial thickness estimated via the Bonart approach for I_b are overestimated slightly. The choice of K and σ does not substantially affect the shape of the final correlation function. Sample calculations suggest that within reasonable upper and lower bounds

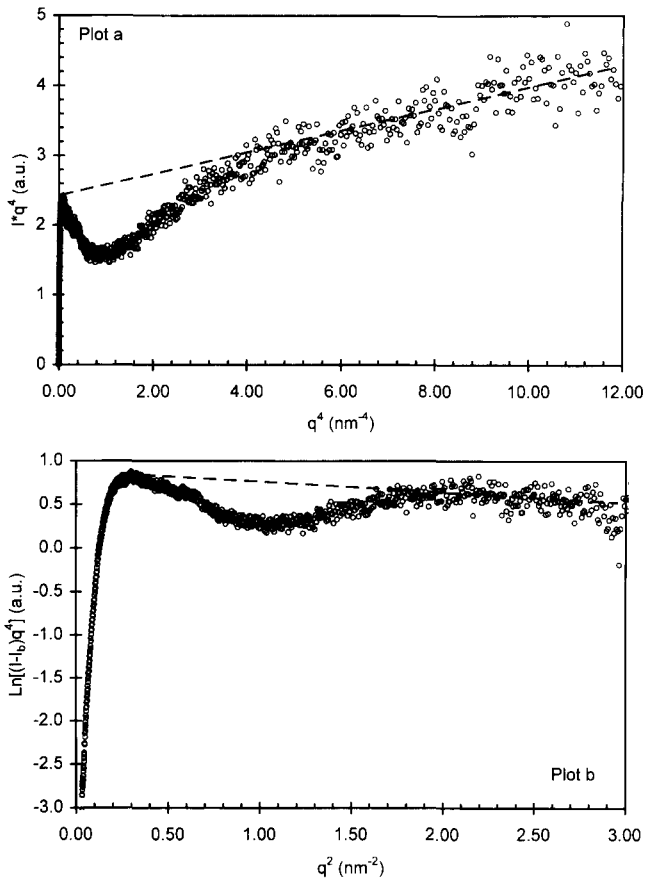

Figure 2 (a) A plot of Iq^4 *versus* q^4 to calculate the Porod law constants K and I_b. K was estimated as the intercept, and I_b was estimated as the slope of the straight line. (b) A plot of $\ln[(I-I_b)q^4]$ *versus* q^2 to refine the Porod law constant K and to estimate σ^2. σ^2 was estimated as the negative slope of the straight line, and K was refined to the exponential of the intercept. Note that the straight line fits are approximations, probably caused by the inadequacies of the Porod region as discussed in the text

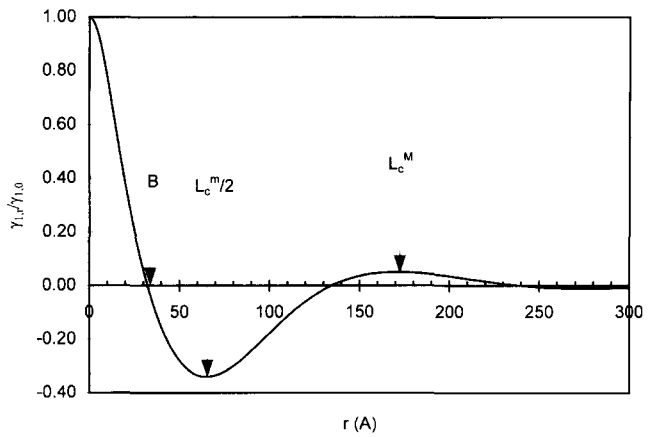

Figure 3 A normalized correlation function typical of all the PEEK samples, and the long spacings extracted from the correlation functions. The long spacing can be estimated as the first maximum (L_c^M) or twice the first minimum (L_c^m). The lamellar thickness can be estimated using equation (4) as discussed in the text

of K and σ, the final lamellar and amorphous layer thickness values did not differ by more than 5%. This observation has also been made by Santa-Cruz *et al.*[25].

The extrapolated data were used to calculate the correlation function as given by equation (1). A typical correlation function is depicted in *Figure 3*. The correlation function was analysed to obtain information on the long period L, linear degree of crystallinity X_{cl}, lamellar thickness l_c, and amorphous layer thickness l_a.

The linear degree of crystallinity X_{cl} was estimated from the correlation function using the two-phase model approach of Strobl and Schneider[20]. If B is the ordinate corresponding to the first zero of the abscissa in the correlation function (see *Figure 3*), and L_c^M is the ordinate corresponding to the first maximum of the abscissa, then

$$X_{cl}(1 - X_{cl}) = \frac{B}{L_c^M} \tag{4}$$

Once the linear degree of crystallinity has been estimated, the average lamellar thickness can be easily estimated as the product of the long spacing and the linear degree of crystallinity. The correlation function can be used to extract two types of long periods: the first maximum (L_c^M) and twice the first minimum (L_c^m) The scattering power (or invariant q) was calculated as the area in the $(I - I_b)q^2$ *versus* q plot extrapolated to low and high q regions. The invariant (Q) can be related to the morphology by the relation given in equation (5)[26]:

$$Q = kX_S X_L[X_{cl}(1 - X_{cl})]\Delta\rho^2 \tag{5}$$

where k is an experimental constant, X_S is the volume fraction of spherulites within the material. X_L is the volume fraction of lamellar stacks within the spherulites, X_{cl} is the linear degree of crystallinity within the lamellar stacks, and $\Delta\rho$ is the (electron) density difference between the crystalline and amorphous phases.

Note that equation (4) will yield two solutions (X_1 and $1 - X_1$) for X_{cl}. It is not possible to mathematically distinguish the value for X_{cl} (between X_1 and $1 - X_1$) based on the SAXS data alone. Several authors including Blundell and Osborn[2], Lee *et al.*[5], and more recently Wang *et al.*[12] and Jonas *et al.*[14,27] suggest that the lower solution of equation (4) corresponds to the correct value for X_{cl}. We disagree with these authors for the following reasons. (1) The average lamellar thickness is expected to increase during melting. As we will demonstrate, only the higher value of X_1 is consistent with this requirement. (2) WAXD patterns of samples with similar thermal histories, when analysed with the Ruland method, suggest an overall degree of crystallinity (X_c) of at least 30%. Since X_{cl} is not expected to be lower than X_c, the lower values of X_1 (which are often less than 0.25) were rejected as being unreasonable. (3) A line broadening analysis of WAXD peaks on PEEK and other similar materials like PEKK 50/50 and new thermoplastic polyimide (n-TPI) result in values for lamellar thicknesses which are only consistent with the higher values for X_{cl}. (Line broadening analysis performed on the 111 peak (assuming infinite dimensions along a and b axes) for alternating PEKK 50/50 crystallized at 260°C without instrumental correction results in a 'lower limit' for lamellar thickness of 80 Å, which was consistent with the higher value of X_{cl} obtained from SAXS. Line broadening analysis performed after instrumental correction on the 001 plane in n-TPI results in values for lamellar thickness which are within 10% of the values calculated using the higher value of X_1 in the correlation function

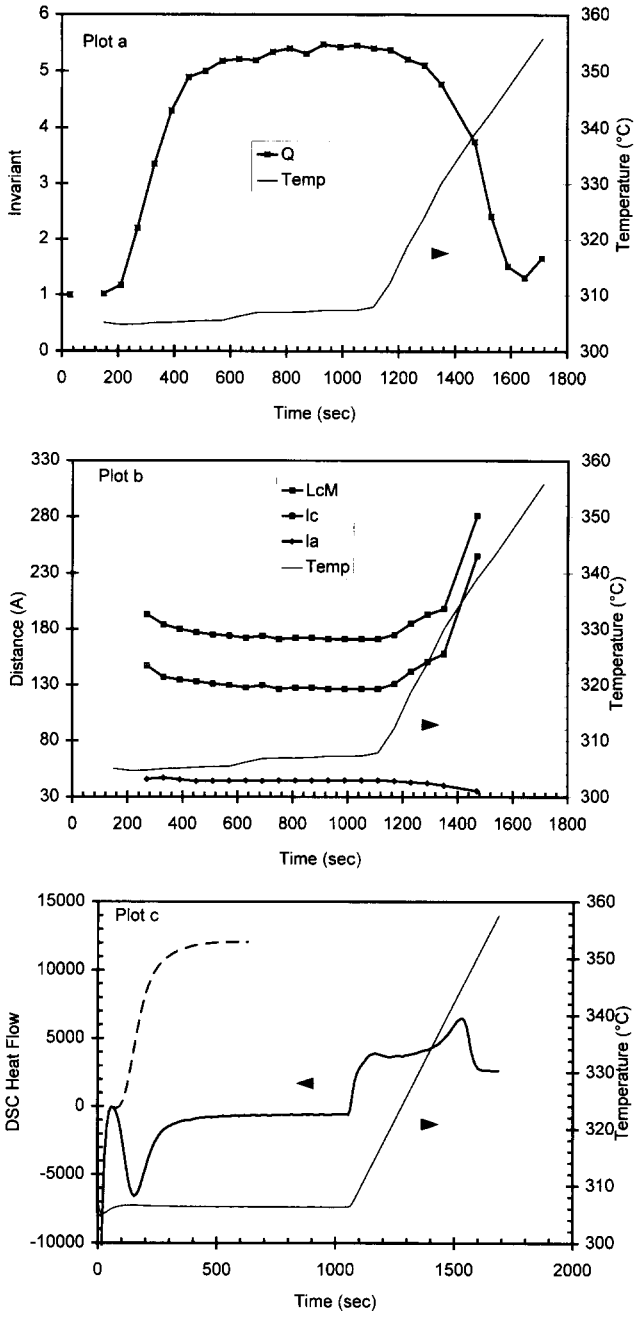

Figure 4 Results of real time SAXS analysis during crystallization at about 307°C followed by melting of PEEK 450G. (a) The scattering invariant (Q) and the temperature *versus* time. (b) The long spacing (L_c^M), the lamellar thickness (l_c) and the amorphous layer thickness (l_a) estimated from the correlation function. (c) A plot of the corresponding d.s.c. traces. This plot includes traces for the temperature (right axes), the d.s.c. heat flow (solid line, left axes), and the integrated d.s.c. heat flow (dashed line, left axes)

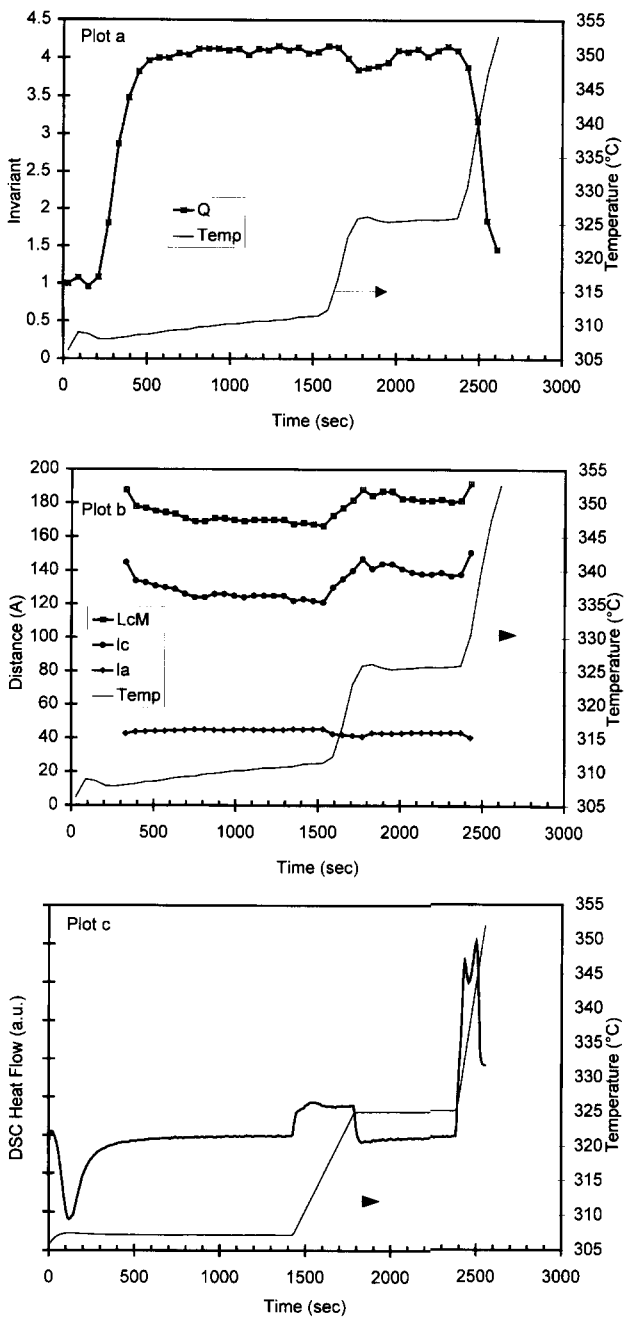

Figure 5 Results of real time SAXS analysis during crystallization at about 307°C followed by a ramp to 323°C, a hold at 323°C and melting of PEEK 450G. (a) The scattering invariant (Q) and the temperature *versus* time. (b) The long spacing (L_c^M), the lamellar thickness (l_c) and the amorphous layer thickness (l_a) estimated from the correlation function. (c) A plot of the corresponding d.s.c. traces. This plot includes traces for the temperature (right axes) and the d.s.c. heat flow (left axes)

approach.) (4) Lovinger *et al.* have used bright field transmission electron microscopy techniques to study the spherulitic morphology in solution crystallized[18] and melt crystallized[19] PEEK. Their work clearly demonstrates that within the lamellar stacks, the lamellar thickness is greater than the amorphous layer thickness (see for example, Figure 5b in ref. 19). Therefore the lamellar thickness was calculated using the larger solution of equation (4) as the value for X_{cl} and the appropriate values of long period (L_c^M).

RESULTS AND DISCUSSION

Figures 4 and *5* summarize the results of morphological studies during melt crystallization and subsequent melting in PEEK. The figures include plots for the invariant (Q) (plot a), and for the lamellar (l_c) and amorphous layer thickness (l_a) and the long spacing (L_c^M) (plot b). D.s.c. traces for similar thermal histories are also provided (plot c). *Figures 4 a–c* depict the results of an isothermal hold at 307°C followed by a slow ramp (heating rate of about 5°C min^{-1} to the melting

temperature. *Figures 5 a–c* depict the results for an isothermal hold at 307°C followed by a ramp to 323°C, an isothermal hold at 323°C and a ramp up to the melting temperature. Note that the two endotherms for isothermal crystallization at 307°C are located at about 312 and 340°C. The temperature for the isothermal hold (323°C) was chosen based on that consideration.

Morphology

The estimated long period (L_c^M) for PEEK crystallized at 307°C is 175 Å. This is higher than the value of 150 Å reported by Hsiao *et al.*[9,10], 157 Å reported by Blundell and Osborn[2] and 148 Å by Lee and Porter[4,5] for PEEK crystallized at 310°C. It is also higher than the long spacing of 143 Å for PEEK crystallized at 320°C reported by Lovinger *et al.*[19] from TEM studies. This discrepancy could potentially be caused by molecular weight difference (Hsiao *et al.* have used PEEK 150G) or by the different analysis techniques used (e.g. the application of Bragg's law by Lee and Porter).

As already mentioned, it is not possible to mathematically distinguish between the two possible solutions for X_{cl}. Our use of the higher solution for X_{cl} results in values of lamellar thicknesses (125 Å for PEEK crystallized at 307°C) substantially higher than those reported by other authors. For example, Blundell and Osborn[2] have reported lamellar thicknesses of 20 Å for PEEK crystallized at 220°C and 48 Å for PEEK crystallized at 310°C. Similar values have also been reported by Lee *et al.*[5] (20 Å for PEEK crystallized at 200°C and 40 Å for PEEK crystallized at 310°C). However, they have estimated the long periods by multiplying the lamellar thickness by the overall degree of crystallinity. Other authors have used the correlation function approach, but used the low value of X_1 for X_{cl}. For example, Wang *et al.*[12] have reported a lamellar thickness of 37.4 Å for PEEK crystallized at 300°C. Jonas and Legras[27] have estimated the lamellar thickness from the Bragg spacing and the overall crystallinity, from the correlation function approach using the lower solution for X_{cl}, and by fitting the raw SAXS data with the general paracrystalline model. They see a reasonable correspondence between the three values for different cold crystallized samples. Their values of lamellar thicknesses are in the 40 Å range for PEEK crystallized at 300°C.

Our rationale for using the higher value for X_{cl} was listed in an earlier section. We would like to further emphasize that the average lamellar thickness is expected to increase during melting. As can be seen from *Figures 4b* and *5b*, the lamellar thickness estimated with the high value of X_{cl} increases during the initial stages of melting. On the other hand, the estimated amorphous layer thickness decreases during the initial stages of melting (see *Figures 4b* and *5b*, and also *Figures 6a* and *6b*). If we had assigned the smaller value of X_1 to X_{cl}, then the estimated lamellar thickness (which would correspond to the amorphous layer thickness of *Figures 6a* and *6b*) would have decreased with increasing temperature during melting. Clearly, such an observation would have violated known physical laws.

Note that using the higher solution for X_{cl} results in X_{cl} being substantially higher than X_c (70% *versus* 35%). This is consistent with the TEM work of Lovinger *et al.*[19]. Their work clearly indicates that within the lamellar stacks of melt crystallized samples, $X_{cl} > 0.5$. An examination of

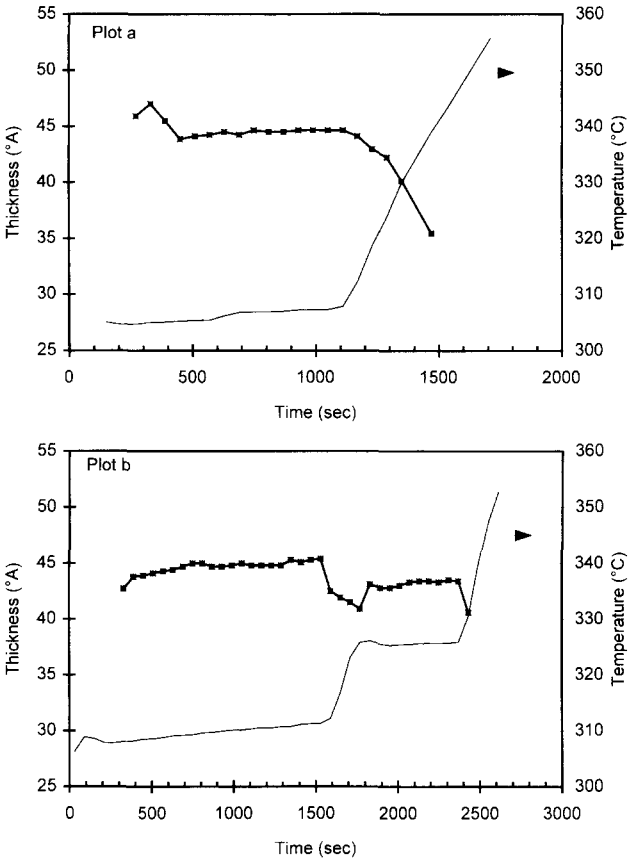

Figure 6 The trends in amorphous layer thickness during the two melting scans. (a) The amorphous layer thickness during isothermal crystallization at 307°C, followed by subsequent melting. (b) The amorphous layer thickness during the isothermal crystallization at 307°C, followed by the ramp to 323°C, and subsequent melting. As discussed in the text, the observed decrease in the amorphous layer thickness implies that melting initiates with 'low melting stacks' composed of thick amorphous layers

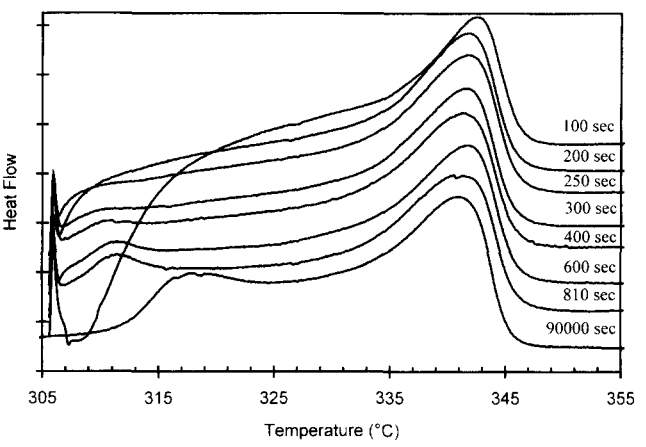

Figure 7 The d.s.c. melting scans for PEEK samples isothermally crystallized at 307°C for different time scales. Note that the d.s.c. traces have been shifted vertically for visual clarity. Also note that the low endotherm develops at later times compared to the high endotherm. This observation contradicts the melting–recrystallization model

the top edge of lamellar stacks depicted in Figure 5 in ref. 19 suggests that the lamellar thickness for PEEK crystallized at 320°C is greater than 100 Å, which is consistent with our calculations. Also, Lattimer *et al.*[15] have reported observing lamellae of thickness 250 Å for

PEEK crystallized at 307°C. They have not monitored the diffraction pattern to account for tilting effects etc. which might result in an overestimation of the lamellar thicknesses. However, their work clearly supports our use of the higher solution of equation (4) for X_{cl}.

Lovinger *et al.*[19] have shown that for PEEK crystallized at 320°C, the spherulites consist of stacks of lamellae, which grow along the crystallographic *b* direction. They estimate the dimension of a typical stack to be about 800–1000 Å, and the spacing of the individual lamellae within the stacks to be about 144 Å. The region between two stacks is amorphous and the spacing between two stacks substantially higher than 800 Å. The scattering technique used in this study is useful in measuring the (electron) density fluctuations in the 15–300 Å range. It is likely that density fluctuations arising from the presence of large interstack amorphous regions have a small effect on the observed SAXS patterns.

Origin of the low endotherm

Trends in the morphological variables depicted in *Figures 4* and *5* clearly suggest that melting initiates immediately upon heating the sample above the crystallization temperature. The question is whether the observed morphological changes are part of one melting–recrystallization phenomenon or whether there is indeed double melting, and if so, can we rule in or rule out the lamellar insertion and lamellar stack models. In this section, we will first test the lamellar insertion model with the experimental observations. We will show that this model is inconsistent with the experimental trends. Next we will show that the melting–recrystallization model is also inconsistent with our observations.

The lamellar insertion model proposes that the low endotherm is caused by melting of thinner lamellae inserted between thicker lamellae. If the model is accurate then upon heating through the low endotherm, the long period, the average lamellar thickness, and the amorphous layer thickness would increase. While the long period and the lamellar thickness do rise during melting (see *Figures 4* and *5*), the amorphous layer thickness decreases (see *Figures 4b*, *5b*, *6a* and *6b*). Therefore, melting of thinner inserted lamellae can be ruled out as an explanation for the low endotherm. Indeed, it can be concluded that melting does not initiate with thinner inserted lamellae. Note that a similar observation was made previously (although not commented on) by Hsiao *et al.*[11].

Additional evidence against the lamellar insertion model can be cited from *Figure 5*. Note that in *Figure 5c*, the disputed low endotherm reappears during annealing at 323°C. This redevelopment of the low endotherm is not accompanied by a decrease in the amorphous layer thickness (see *Figures 5b* and *6b*), as would have been expected by the insertion of thinner lamellae between thicker ones.

Figure 7 depicts d.s.c. melting scans of isothermally melt crystallized ($T_c = 307$°C, varying t_c as indicated on the traces) PEEK samples. If the melting–recrystallization model had been accurate, then the development of the high endotherm would not have preceded that of the low endotherm. The d.s.c. scans of *Figure 7* indicate that the high endotherm develops first, and that the low endotherm develops subsequently and continues to develop at time scales greater than 400 s. Similar results have been obtained by Velikov and Marand[16]. Clearly, such an observation is incompatible with the melting–recrystallization model.

To summarize: (1) evidence has been presented which discounts the lamellar insertion model as an explanation for the low endotherm; (2) a combination of d.s.c. and SAXS techniques suggests that the melting–recrystallization model is also inadequate in explaining the low endotherm. These conclusions, in conjunction with the definitive work of Krüger and Zachmann[13], suggest that the finite lamellar stack model accurately describes the morphology of PEEK.

Morphological changes during crystallization and melting

In the last section, we suggested that the origin of the low endotherm lies in the melting of stacks of thin lamellae. In this section, we report studies of the initiation of melting in more detail. This has been done (1) by comparing the morphological variables (L_c^M, l_a and l_c) extracted from the correlation function, and (2) by examining the trends in the two correlation function long spacings in light of modelling results discussed earlier in this paper, and of the results presented by Santa-Cruz *et al.*[25].

In the last section, it was suggested that melting initiates with 'low melting stacks' of thinner lamellae. In order to be consistent with the observed decrease in average amorphous layer thickness during melting (see *Figures 6a* and *6b*), the low melting stacks must have a higher amorphous layer thickness than the high melting stacks. This places an additional constraint on the low melting stacks. Based on these observations, we suggest that the low endotherm results from melting of stacks composed of thin lamellae and thick amorphous layers.

Melting of such low melting stacks would decrease the variance in lamellar thickness distribution (σ_c). The work of Santa-Cruz *et al.*[25] suggests that (when $X_{cl} > 0.5$) $L_c^M > L_c^m$ if $\sigma_c > \sigma_a$. Also, when $\sigma_c < \sigma_a$, then $L_c^m > L_{true}$. Therefore (for our case, where $X_{cl} > 0.5$), if σ_c/σ_a were to decrease, then L_c^M and L_c^m would converge. *Figures 8a* and *8b* summarize the L_c^m and L_c^M values during the two experiments. As can be seen clearly from *Figures 8a* and *8b*, L_c^m and L_c^M converge during crystallization, but diverge during melting. The divergence of the two long spacings during melting implies that σ_c/σ_a must increase. Since σ_c must necessarily decrease with melting of thinner lamellar, σ_a must decrease at a faster rate. Clearly, this last observation is consistent with the additional constraint of thicker amorphous layers placed on the low melting stacks.

Note that the proposed model for initiation of melting is consistent with the open and coarse type of spherulites reported at high crystallization temperatures by several authors[19,28]. As the crystallization temperature is lowered, the spherulitic morphology becomes compact and finer. For example, Hudson *et al.*[28] have studied the morphology of spherulites crystallized from blends of PEEK and a poly(ether imide) (Ultem). They have quantified the coarseness with a scale of aggregation, which they have defined as the sum of the average lamellar bundle and amorphous pocket widths. They have shown that for a 75% PEEK

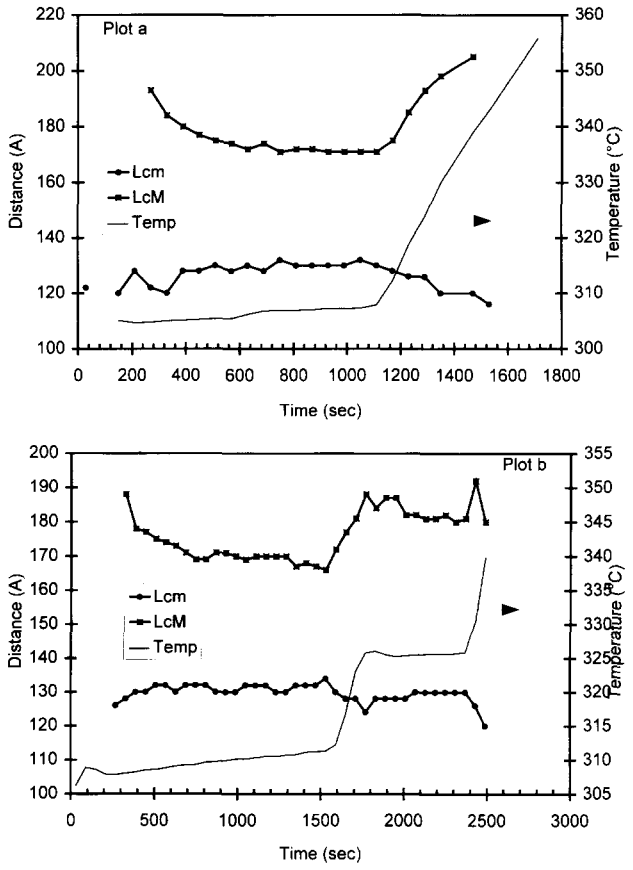

Figure 8 The properties of the correlation function during crystallization and subsequent melting. The plots include traces for twice the first minimum (L_c^m), and for the first maximum (L_c^M). (a) L_c^m and L_c^M during isothermal crystallization at 307°C, followed by melting. (b) L_c^m and L_c^M during isothermal crystallization at 307°C, followed by a ramp to 323°C, and subsequent melting. As discussed in the text, the divergence of the two estimates during melting further confirms that melting initiates with stacks comprising of thick amorphous layers

blend, for crystallization temperatures of 300, 270 and 250°C, the scale of aggregation decreases from 1200 to 600 to 400 nm respectively. Therefore, for PEEK crystallized at lower temperatures (with more compact and finer spherulites), we would expect melting to initiate differently. These aspects will be discussed in future publications.

To summarize, we propose that for high crystallization temperatures, melting initiates with low melting stacks of thinner lamellae and thicker amorphous layers. This type of melting results in a decrease in the variance of both the lamellar and amorphous size distributions and the average amorphous layer thickness, while increasing the average lamellar thickness.

CONCLUSION

The morphological developments in PEEK during melt crystallization and heating above the crystallization temperature have been studied using real time SAXS. The correlation function approach has been used to extract trends in the morphological details at the lamellar level. While long spacings and lamellar thicknesses calculated in this study are higher than those reported by other authors, the discrepancy has been assigned to the different approaches used for data analysis.

The amorphous layer thickness has been observed to decrease during initial stages of melting. From this observation, melting of thin inserted lamellae can be ruled out as an explanation for the low endotherm and as a possible explanation for the initiation of melting. Also, a combination of SAXS and d.s.c. techniques suggests that the melting–recrystallization model is flawed. Based on these observations, and the previous work of Krüger and Zachmann, we suggest that the origin of the low endotherm lies in the melting of discrete stacks of thin lamellae. These stacks of secondary lamellae form subsequent to the stacks of thick primary lamellae.

Lastly, from the observed decrease in the amorphous layer thickness during melting, and the divergence of the two correlation function long spacings, it is proposed that melting initiates with low melting stacks of thinner lamellae and thicker amorphous layers. We speculate that these low melting stacks correspond to the stacks of thinner lamellae that are formed during the so-called secondary crystallization stage.

ACKNOWLEDGEMENTS

This study was made possible by generous financial support of several organizations. We gratefully acknowledge DuPont CR&D for their financial assistance and donation of synchrotron beamtime. Additional support was provided by the NSF Science and Technology Center under DMR grant 91-2004. H.M. would also like to thank the National Science Foundation for the Young Investigator Award (DMR 93-57512). Excellent technical assistance was provided by Mr Joe McKeown. We acknowledge the critical and helpful discussions with Dr Alain Jonas, Dr Do Yoon and Dr T. P. Russell. Thanks are also due to Dr Garth Wilkes and Mr Srinivas Srivatsan for helpful comments and suggestions.

REFERENCES

1 Holdsworth, P. J. and Turner-Jones, A. *Polymer* 1971, **12**, 195
2 Blundell, D. J. and Osborn, B. N. *Polymer* 1983, **24**, 953
3 Blundell, D. J. *Polymer* 1987, **28**, 2248
4 Lee, Y. and Porter, R. S. *Macromolecules* 1987, **20**, 1336
5 Lee, Y., Porter, R. S. and Lin, J. S. *Macromolecules* 1989, **22**, 1756
6 Cheng, S. Z. D., Cao, M. Y. and Wunderlich, B. *Macromolecules* 1986, **19**, 1868
7 Cebe, P. and Hong, S. D. *Polymer* 1986, **27**, 1183
8 Bassett, D. C., Olley, R. H. and Raheil, I. A. M. *Polymer* 1988, **29**, 1745
9 Hsiao, B. S., Gardner, K. H., Wu, D. Q., Liang, B. and Chu, B. *ACS Polym. Prepr.* 1992, **33**, 265
10 Hsiao, B. S., Gardner, K. H., Wu, D. Q. and Chu, B. *Polymer* 1993, **34**, 3986
11 Hsiao, B. S., Gardner, K. H., Wu, D. Q. and Chu, B. *Polymer* 1993, **34**, 3996
12 Wang, J., Alvarez, M., Zhang, W., Wu, Z., Li, Y. and Chu, B. *Macromolecules* 1992, **25**, 6943
13 Krüger, K.-N. and Zachmann, H. G. *Macromolecules* 1993, **26**, 5202
14 Jonas, A., Russell, T. P. and Yoon, D. *Macromolecules* 1995, **28**, 8491
15 Lattimer, M. P., Hobbs, J. K., Hill, M. J. and Barham, P. J. *Polymer* 1992, **33**, 3971
16 Velikov, V. and Marand, H. *Macromolecules* preprint
17 Marand, H. and Prasad, A. *Macromolecules* 1992, **25**, 1731
18 Lovinger, A. J. and Davis, D. D. *Macromolecules* 1986, **19**, 1861

19 Lovinger, A. J., Hudson, S. D. and Davis, D. D. *Macromolecules* 1992, **25**, 1752
20 Strobl, G. R. and Schneider, M. *J. Polym. Sci., Polym. Phys. Edn.* 1980, **18**, 1343
21 Koberstein, J. T. and Stein, R. S. *J. Polym. Sci., Polym. Phys. Edn.* 1983, **21**, 2181
22 Bonart, R. and Muller, E. H. *J. Macromol. Sci. Phys.* 1974, **B10**(1), 177
23 Vonk, G. G. *J. Appl. Cryst.* 1973, **6**, 81
24 Ruland, W. *Colloid Polym. Sci.* 1977, **255**(5), 417
25 Santa-Cruz, C. S., Stribeck, N., Zachmann, H. G. and Calleja, B. J. *Macromolecules* 1991, **24**, 5980
26 Glatter, O. and Kratky, O. 'Small Angle X-Ray Scattering', Academic Press, London, 1982
27 Jonas, A. and Legras, R. *Macromolecules* 1993, **26**, 813
28 Hudson, S. D., Davis, D. D. and Lovinger, A. J. *Macromolecules* 1992, **25**, 1759